RSC Advances

This is an *Accepted Manuscript*, which has been through the Royal Society of Chemistry peer review process and has been accepted for publication.

Accepted Manuscripts are published online shortly after acceptance, before technical editing, formatting and proof reading. Using this free service, authors can make their results available to the community, in citable form, before we publish the edited article. This *Accepted Manuscript* will be replaced by the edited, formatted and paginated article as soon as this is available.

You can find more information about *Accepted Manuscripts* in the Information for Authors.

Please note that technical editing may introduce minor changes to the text and/or graphics, which may alter content. The journal's standard Terms & Conditions and the Ethical guidelines still apply. In no event shall the Royal Society of Chemistry be held responsible for any errors or omissions in this *Accepted Manuscript* or any consequences arising from the use of any information it contains.

ROYAL SOCIETY OF CHEMISTRY

www.rsc.org/advances

Please do not adjust margins

Journal Name

ARTICLE

Hierarchical $LiMnPO_4$ assembled from nanosheets via solvothermal method as high performance cathode material

Received 00th January 20xx,
Accepted 00th January 20xx

DOI: 10.1039/x0xx00000x

www.rsc.org/

Zhijian Zhang[1], Guorong Hu[1], Yanbing Cao [1*], Jianguo Duan[1], Ke Du[1], Zhongdong Peng[1]

A series of $LiMnPO_4$ nanoparticles with different morphology have been successfully synthesized via solvothermal method. The samples have been characterized by X-ray diffraction (XRD), Scanning electron microscope (SEM), Transmission electron microscopy (TEM). The results show that morphology, particle size and crystal orientation are controllable synthesized by various precursor composite tailoring with various Li:Mn:P molar ratio. At 3:1:1, Li^+-containing precursor Li_3PO_4 is obtained while at 2:1:1, only Mn^{2+}-containing precursor involving $Mn_5(PO_4)_2[(PO_3)OH]_2{\cdot}4H_2O$ and $MnHPO_4{\cdot}2.25H_2O$ is detected. Specially, at 2.5:1:1, the precursor consists predominantly of Mn^{2+}-containing precursor with minor amount of Li_3PO_4. From 2:1:1 to 3:1:1, the particle morphology evolves from sheet to spherical texture accompanied with the particle size reduced. In the presence of urea, highly uniform $LiMnPO_4$ with hierarchical micro-nanostructure is obtained, which is composed of nanosheets with the thickness of several tens of nanometers. Thus, those unique hierarchical nanopartilces with open porous structure play an important role in $LiMnPO_4$ cathode material. At the concentration of 0.16 mol L^{-1} for urea, the hierarchical $LiMnPO_4$/C sample assembled from nanosheets with (010) facet exposed shows the best electrochemical performance, delivering higher reversible capacity of 150.4, 142.1, 138.5, 125.5, 118.6 mAh g^{-1} at 0.1, 0.2, 0.5, 1.0, 2.0C, respectively. Moreover, the composites show long cycle stability at high rate, displaying a capacity retention up to 92.4% with no apparent voltage fading after 600 cycles at 2.0 C.

1. Introduction

$LiMnPO_4$ is one of the most promising cathode material for lithium ion-batteries, due to its high specific capacity, low toxicity, low cost, and excellent thermal stability, and has been expected to be applied in a wide-scale use in plug-in hybrid electric vehicles (PHEVs), electric vehicles (EVs) and smart grid storage that fast electronic transfer and superior ionic migration are demanded.[1, 2] However, the bulk $LiMnPO_4$ suffers from poor electronic conductivity and slow Li^+ diffusion, leading to low specific capacity, poor rate capacity, and inferior cycle stability.[3-5] Up to now, the electrochemical performance of $LiMnPO_4$ cathode material has been improved by controlling the particle size and morphology. It has been demonstrated that the particles with dimensionally modulated nanostructure such as nanorod, nanosheets and nanosphere can enhance the electrochemical performance due to a shortening of both the electron and lithium ion diffusion path lengths within the particles.[6-8] The cluster-like $LiMnPO_4$ composed of nanoplates with a thickness of ca. 35 nm and a width of ca. 400 nm via a solvothermal method exhibited a discharge capacity of 147 mAh g^{-1} at 0.05 C.[9] Xu et.al. reported the rod-like $LiMnPO_4$ via a solvothermal method, showing a reversible capacity of 153.4 mAh g^{-1} at 0.1 C, which is ascribed to the nanostructure with the average length and diameter of approximately 100 and 60 nm, respectively.[10] In this sense, the nanostructure is key to synthesizing $LiMnPO_4$ cathode material with excellent electrochemical performance. Since the solvothermal process is a facile approach to prepare nanostructure and high crystalline materials with the notable virtues such as simple and straight ward operations, cost-effectiveness, and scalable production, it has been widely used to prepare the $LiMnPO_4$ cathode material. So far, nanostructured $LiMnPO_4$ cathode material has been successfully prepared via the solvothermal process, in which the expensive chemicals was used.[11, 12] What's more, in a traditional hydrothermal/solvothermal method, to prepare the nanostructured $LiMnPO_4$, excess Li is used with the Li:Mn:P molar ratio of 3:1:1 or even more.[12, 13] Up to now, EG based solvent has been successfully used to prepare micro- and nano-structure $LiMPO_4$ (M=Fe, Mn, Ni) for lithium ion-batteries, and the morphology could be easily tuned by altering the synthesis condition or selecting different raw materials, such as the concentration, solvent, temperature and time, pH valve, feeding sequence and the surfactant.[6, 8, 14-18] However, It is rarely reported the effect of the phase composition in the precursor solution or Li:Mn:P molar ratio on the morphology and structure of $LiMnPO_4$. Thus, it deserves further research to reveal the role that phase composition or Li:Mn:P molar ratio play in the preparation of $LiMnPO_4$. With this perspective, we

[1]School of Metallurgy and Environment, Central South University, Changsha 410083, China. E-mail address: cybcsu@csu.edu.cn; Tel: +86-13875868540; Fax: +86-0731-88830474.
†Electronic Supplementary Information (ESI) available: [details of any supplementary information available should be included here]. See DOI: 10.1039/x0xx00000x

RSC Advances Accepted Manuscript

report the morphology controllable synthesis of $LiMnPO_4$ tailoring with the molar ratio of Li:Mn:P by solvothermal method, using ethanol as green solvent, LiH_2PO_4, $LiOH \cdot H_2O$ and $MnSO_4 \cdot H_2O$ as the starting material, as illustrated in Scheme 1.

On the other hand, it is hard to control the morphology, especially for highly uniform particles with nanostructure. Generally, the nanoparticles prefer to agglomerate together, which in turn constantly limits the demonstration of its intrinsic performance. In this regard, $LiMnPO_4$ nanoparticles with a novel hierarchical micro-nanostructure are expected as a new prototype to minimize the self-agglomeration and re-stacking and also facilitate physical properties at macroscale.

Herein, a urea assisted solvothermal method was proposed for the growth of hierarchical micro-nanostructured $LiMnPO_4$ by controlling the molar ratio of Li:Mn:P at 2:1:1. To fully demonstrate the effect of urea, the concentration of urea was optimized. With the morphology and composition advantages, the as-prepared $LiMnPO_4$/C is expected to manifest superior electrochemical performance, especially, the high rate capacity and long cycle stability.

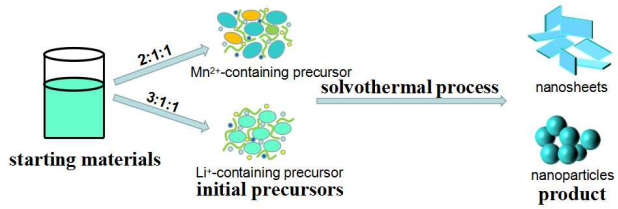

Scheme. 1 the morphology controllable solvothermal process by tailoring with the Li:Mn:P molar ratio

2. Experimental

2.1 preparation

The $LiMnPO_4$ samples were prepared by solvothermal approach in ethylene glycol (EG) and de-ionized water mixing solvent (volume ratio of 9:1) as follows: various amount of LiOH aqueous solution was added drop-wise into the LiH_2PO_4 EG-H_2O solution under vigorous stirring, and then CTAB (hexadecyl trimethyl ammonium bromide, 0.015 mol L^{-1}) was dissolved in the above white suspension followed by $MnSO_4$ aqueous solution introduced into the mixture. The final mixture was transferred to a 300 mL stainless steel autoclave. The concentration of Mn^{2+} in the precursor solution was controlled to be 0.1 mol L^{-1}. The solvothermal reaction was carried out at 220 ℃ for 4 h to form a white precipitation. After that, white particles were collected via centrifugation, washed with distilled water three times, absolute ethanol twice. After dried in a vacuum oven at 60 ℃ for 12 h, the as-prepared $LiMnPO_4$ was mixed and ground with PVA (20 wt%), and then annealed at 670 ℃ for 4 h (3 ℃/min) under an Ar atmosphere to carbonize glucose and increase the crystallinity of the $LiMnPO_4$ material. The mass percentage of carbon was determined by carbon sulfur analyzer to be about 3.4 wt%. The molar ratio of Li:Mn:P was controlled at 2:1:1, 2.5:1:1 and 3:1:1 by adjusting the added amount of LiOH, and the product was named s-1, s-2 and s-3. During the series experiments in the presence of urea, the molar ratio of Li:Mn:P was 2:1:1, while the concentration of urea was controlled at 0.08, 0.12, 0.16, 0.2 mol L^{-1}, namely s-4, s-5, s-6, and s-7, respectively.

2.2 Characterization

The crystal structures of the synthesized powers were examined by X-ray diffraction (XRD) (Haoyuan DX-2500, Dandong Instrument Co., Ltd., China) analysis with nickel-filtered Cu $K\alpha$ radiation (λ= 1.5418 Å) over the 2θ range from 10° to 90° . The morphology was investigated with a field emission scan electron microscope (SEM, JEOL JSM-6360LV, and Japan) and a transmission electron microscope (TEM, Tecnai G2 F20).

2.3 Electrochemical measurement

The electrochemical performance of the samples as cathode material was evaluated using CR2025 coin cells assembled in an argon-filled glove box. For the cathode preparation, a mixture of $LiMnPO_4$/C, Super P carbon, and poly(vinyl difluoride) (PVDF) with a weight ratio of 75:15:10 was pasted on an Al foil, which works as a current collector. A Celgard 2340 microporous membrane was used as the separator and lithium foil was used as the counter electrode. The non-aqueous electrolyte was 1 M $LiPF_6$ solution in ethylene carbonate, dimethyl carbonate, and methyl-ethyl carbonate with a volume ratio of 1:1:1 (LIB 315, Guotai Huarong Chem. Co., Ltd., Zhangjiagang, China). The electrochemical tests were carried out at room temperature on a Land Test System (CT2001A, Wuhan Jinnuo Eletronic Co., Ltd., Wuhan China) setting the cut off voltages of 2.50~4.50 V versus Li^+/Li (1 C=160 mA g^{-1}).

3. Results and discussion

3.1 effect of Li:Mn:P molar ratio

The structure and morphology of the product are highly dependent on the Li:Mn:P molar ratio. The XRD pattern of the product obtained from various molar ratio are presented in Fig. 1. It can be clearly seen that all samples are single phase which can be indexed to the orthorhombic olivine structure with a *Pmnb* space group (JCPDS card no.74-0375). Upon closer observation, the relative peak intensities change with the molar ratio variation of Li:Mn:P. The diffraction intensity from the (020) facet is strongest at 2:1:1, while the highest intensity at 3:1:1 comes from the (311) facet. This may indicate that the as-obtained sample at 2:1:1 has a preferential crystal orientation along the [010] direction, which is favorable to the Li^+ diffusion due to the fact that $LiMnPO_4$ has a one-dimension migration path along the b axis.[9, 19] Fig. 2 shows the SEM images of the samples tailoring with different Li:Mn:P molar ratio. At 2:1:1, a novel morphology was obtained. As shown in Fig. 2a, the sample consists of sheet-like crystals with the thickness of several tens of nanometers, a mean length of ~450 nm, an average width of ~300 nm, in which the small crystals attach together irregularly to assemble into hierarchical structure with open porousness. But

RSC Advances Accepted Manuscript

This journal is © The Royal Society of Chemistry 20xx

unfortunately, the hierarchical structure is not open enough, thus we carried out the urea assisted solvothermal method to effectively take advantage of those novel morphology which will be discussed later in detail. When the molar ratio is prolonged to 2.5:1:1, $LiMnPO_4$ composed of sheet-like crystals similar to 2:1:1 is obtained. It is clearly seen that the obtained sample was randomly dispersed with well-defined shape, in which the sheet-like crystals have a uniform particle size distribution. For instance, the length is varied from 250 nm to 500 nm, while the width from 150 nm to 450 nm. When the molar ratio increased to 3:1:1, the particles are near-spherical with an average diameter of several tens of nanometers. Obviously, the particles are seriously agglomerated, which will bring negative effects on the electrochemical performance. It is worth noting that, when increasing the molar ratio of Li:Mn:P, a smaller particle size is achieved, indicating that excess Li was favorable for attaining small particle size for $LiMnPO_4$, in well agreement with the previous study.[20, 21]

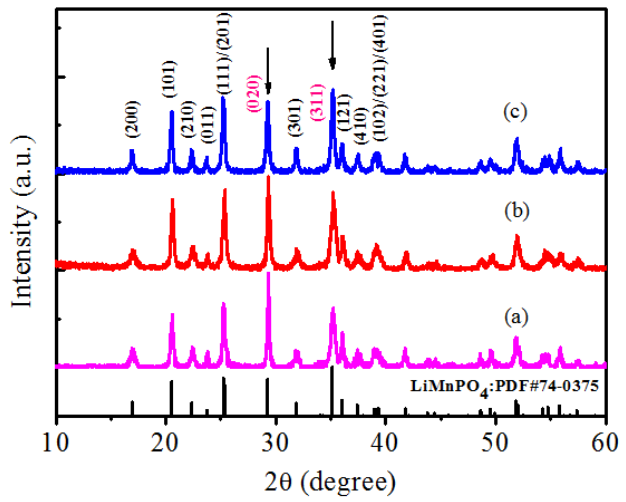

Fig. 1 the XRD pattern of the sample tailoring with different Li:Mn:P molar ratio: (a) 2:1:1; (b)2.5:1:1; (c) 3:1:1.

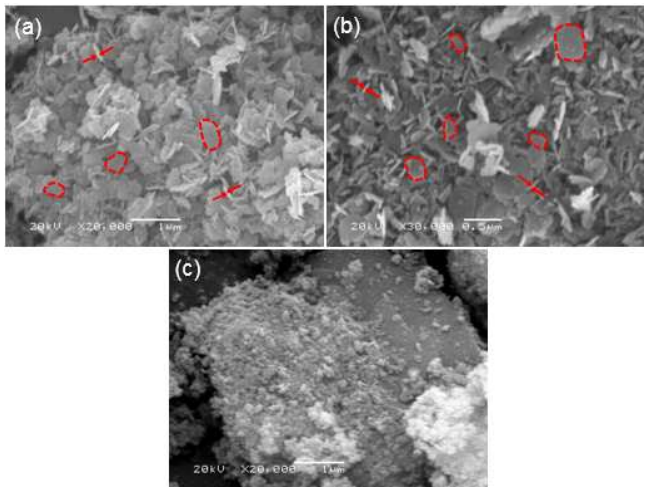

Fig. 2 the SEM images of samples tailoring with different Li:Mn:P molar ratio: (a) 2:1:1; (b)2.5:1:1; (c) 3:1:1.

To further understand the evolution of morphology and the diversity of particle size. The structure and morphology of the precursors from the mother solution before solvothermal treatment were characterized. The XRD patterns of the dried precursors synthesized at room temperature are presented in Fig.3. The phase composition of the precursor is strongly affected by the molar ratio of Li:Mn:P. From the XRD patterns, obviously, Mn^{2+}-containing precursor involving $Mn_5(PO_4)_2[(PO_3)OH]_2{\cdot}4H_2O$ (JCPDS card no.34-0146) and $MnHPO_4{\cdot}2.25H_2O$ (JCPDS card no.47-0199) is stable at the off-stoichiometry, leaving Li^+ freely existing in the mother solution, as the molar ratio of Li:Mn:P increased, Li_3PO_4 phase (JCPDS card no.25-1030) is detected. When increased to 3:1:1, no other phase but Li^+-containing precursor Li_3PO_4 is identified, while the manganese salt phases cannot be detected. Fig. S1 shows the SEM images of the dried precursors, clearly, at 3:1:1, the particles exhibit spherical texture similar to that of the resultant product $LiMnPO_4$, indicating that $LiMnPO_4$ is most likely formed by an in situ evolution from the precursor Li_3PO_4 in the solvothermal method, in agreement with previous research.[22] In the EG based solvothermal condition in which water is almost highly deficient is not likely able to dissolve the starting material Li_3PO_4 to form the intermediate phases such as $Mn_3(PO_4)_2$, $MnHPO_4$, which are known as the dissolution-reprecipitation process in the hydrothermal method similar to $LiFePO_4$,[23, 24] Thus, the Li_3PO_4 may plays as an hard template to form $LiMnPO_4$ directly. At 2:1:1, the precursor also presents the spherical texture different with the subsequent product, which may due to the multi-phases in the precursor solution, in which case the crystal units may contain more than one nucleus with different orientation and growth rates. In addition, such remarkable divergence in precursor solution results in different released ions from the precursor with various types or priority orders, leading to the different nucleation or growth rates. In this regard, the distinction in morphology is caused by the different solution composition generated by adjusting the molar ratio of Li:Mn:P.

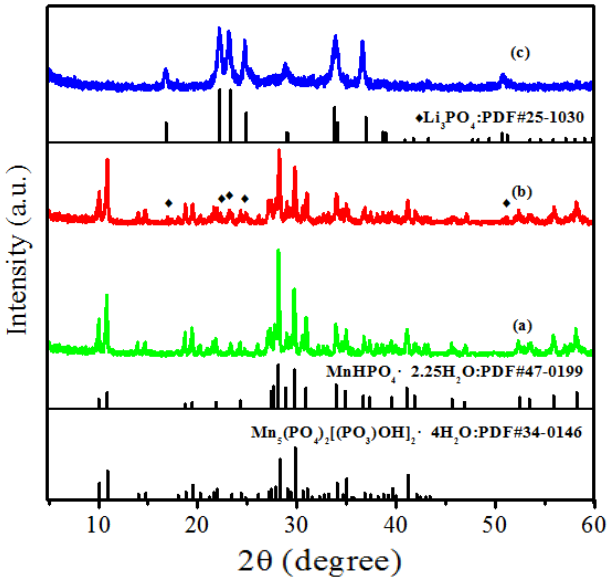

Fig. 3 the XRD pattern of the precursors tailoring with different Li:Mn:P molar ratio: (a) 2:1:1; (b)2.5:1:1; (c) 3:1:1.

RSC Advances Accepted Manuscript

Based on the above results, it can be reasonably understood that the molar ratio of Li:Mn:P has a great effect on the phase composition of the precursor, which will control the morphology and particle size of the $LiMnPO_4$ crystals in the solvothermal process. To further confirm the roles of molar ratio of Li:Mn:P, also, taking advantage of the sheet-like crystals with preferred orientation of [010] direction, a set of independent experiments were carried out where urea was mainly used as the alkaline reagent.

3.2 effect of urea addition

Crystal structure is significantly important for cathode materials, including the phase composition, crystallinity, and crystal orientation. To characterize the crystal structure of $LiMnPO_4$, the series samples were tested by XRD after thermal treatment. Fig. 4 shows the XRD pattern of the series samples. Among the samples after thermal treatment, the diffraction peaks can be well indexed to the orthorhombic olivine type $LiMnPO_4$ (JCPDS card no.74-0375), and no other impurity phase is found except that of the sample s-7, in which the impurity phase Mn_3O_4 (JCPDS card no.24-0734) is observed. In addition, the sample s-7 before thermal treatment, the impurity phase MnO_2 (JCPDS card no.12-0141) is detected. Thus, the formation of Mn(IV) impurity may be caused by the oxidation of Mn^{2+} with oxygen from the solution and air in the dissolving and feeding processes, because Mn^{2+} is strongly sensitive to the oxygen in a strong alkaline environment due to the increasing amount of urea. Also, the similar results are found in $LiFePO_4$ under the hydrothermal/solvothermal condition.[25-27] Under the thermal treatment, the MnO_2 was further reduced by the decomposed carbon to form Mn_3O_4. Therefore, excess urea would cause the side reaction, leading to impurity phase. It is worth noting that all the samples are well crystallized with the strongest peak (020), indicating an enlarged (010) facet exposed is expected.

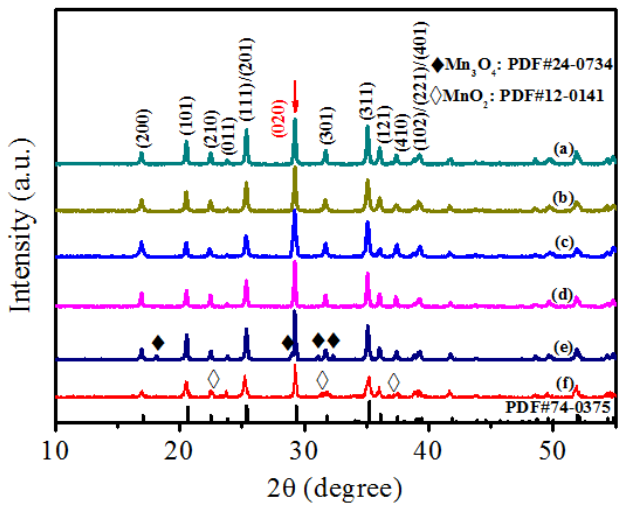

Fig. 4 the XRD pattern of the samples with various concentration of urea under thermal treatment: (a) 0 mol L^{-1}; (b) 0.08 mol L^{-1}; (c) 0.12 mol L^{-1}; (d) 0.16 mol L^{-1}; (e) 0.2 mol L^{-1}; (f) 0.2 mol L^{-1} without thermal treatment

According to the SEM images in Fig. 5, the morphologies are not obviously changed by varying the concentration of urea, and all the samples are composed of sheet-like crystals, which indicates that urea can act as an alkaline reagent for the formation of $LiMnPO_4$ phase and has no obvious role in changing the shape of the $LiMnPO_4$ crystals. Therefore, it is believed that the phase composition of the precursor has a great effect on the morphology of $LiMnPO_4$ instead of the pH when tailoring with the molar ratio of Li:Mn:P. In addition, the $LiMnPO_4$ crystals assemble regularly to form the flower-like structure with more open porousness gradually, as increasing the concentration of urea. For the closed observation in Fig. 5, we can see that the particle size become smaller with the increasing amount of urea, as well as less agglomeration, indicating that urea is useful to reduce agglomeration and inhibit particles from growing. Importantly, when the concentration of urea is increased to 0.16 mol L^{-1}, the sample consists of nanosheets with flower-like texture. As shown in Fig. 6a-c, the flower-like sample is uniformly dispersed with well-defined micro-nanostructure. Obviously, the nanosheets crosslink together forming an open porous structure with an average thickness of several tens of nanometers, which further demonstrates their loose-packed flowery architecture. From the Fig. 6d, it is clear that the hierarchical structure can be maintained after the thermal treatment, which may be due to the fact that the relative low calcination temperature and short calcination time was employed during the thermal treatment, also the decomposed carbon can hinder agglomeration. Thus, those highly hierarchical structure constructed from the attached sheet-like crystals is beneficial to reduce the transport lengths for both electron and ion for the large surface areas readily accessible to electrolyte compared with the bulk material. Furthermore, the micro-nanostructure enables easy operation in terms of electrode fabrication and high tap density, compared with the nanoparticles. In addition, from the HRTEM image in Fig. 6e, the sample exhibits a set of lattice fringe with the d spacing value of 0.43 nm, which is indexed to the (101) facet of $LiMnPO_4$. Importantly, the sample has a uniform and perfect carbon coating on the surface of $LiMnPO_4$ with a thickness of around 2 nm, which is beneficial to the electron transfer. It also reveals that the flower-like sample is a single crystal from the clear lattice fringe, which is further confirmed by the FFT pattern with regular spots. A more detailed analysis of FFT pattern reveals that the sample exhibits an exposed (010) as shown in Fig. 6f. Combination the XRD,TEM, HRTEM and FFT pattern, we could further confirm that the b axis of the sheet-like crystals are parallel to the electron beam direction [010], indicating that the product of the flower-like sample exposes a large (010) facet and the [010] direction is the thinnest direction of the particle, which is an optimal situation for $LiMPO_4$ (M=Mn, Fe) cathode material with favorable lithium ion migration owing to the known fact that lithium (de)insertion in $LiMPO_4$ (M=Mn, Fe) is along the b-axis.[28, 29]

RSC Advances Accepted Manuscript

This journal is © The Royal Society of Chemistry 20xx

Please do not adjust margins

Journal Name

ARTICLE

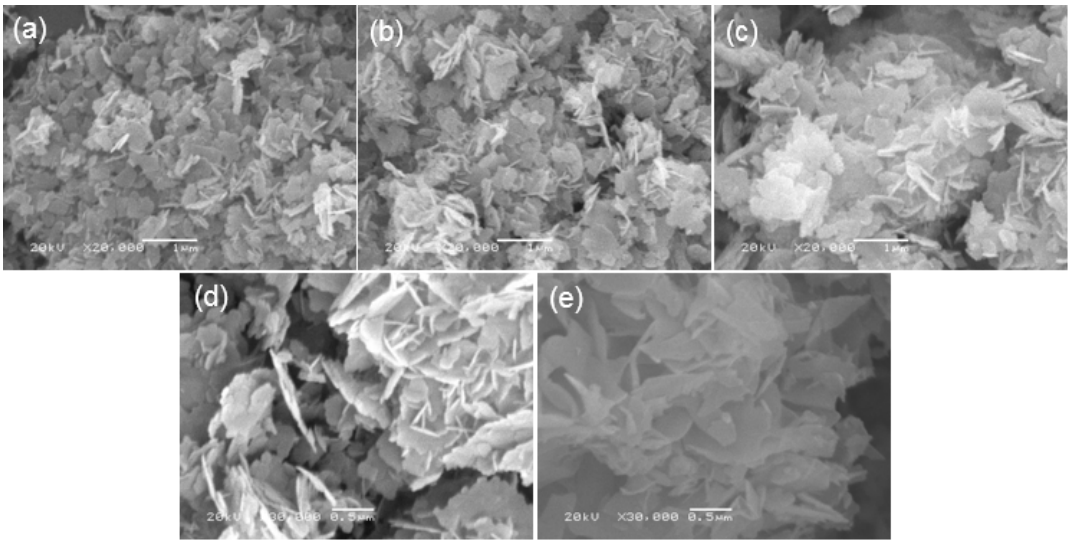

Fig. 5 the SEM images of the samples with various concentration of urea: (a) 0 mol L^{-1}; (b) 0.08 mol L^{-1}; (c) 0.12 mol L^{-1}; (d) 0.16 mol L^{-1}; (e) 0.2 mol L^{-1}

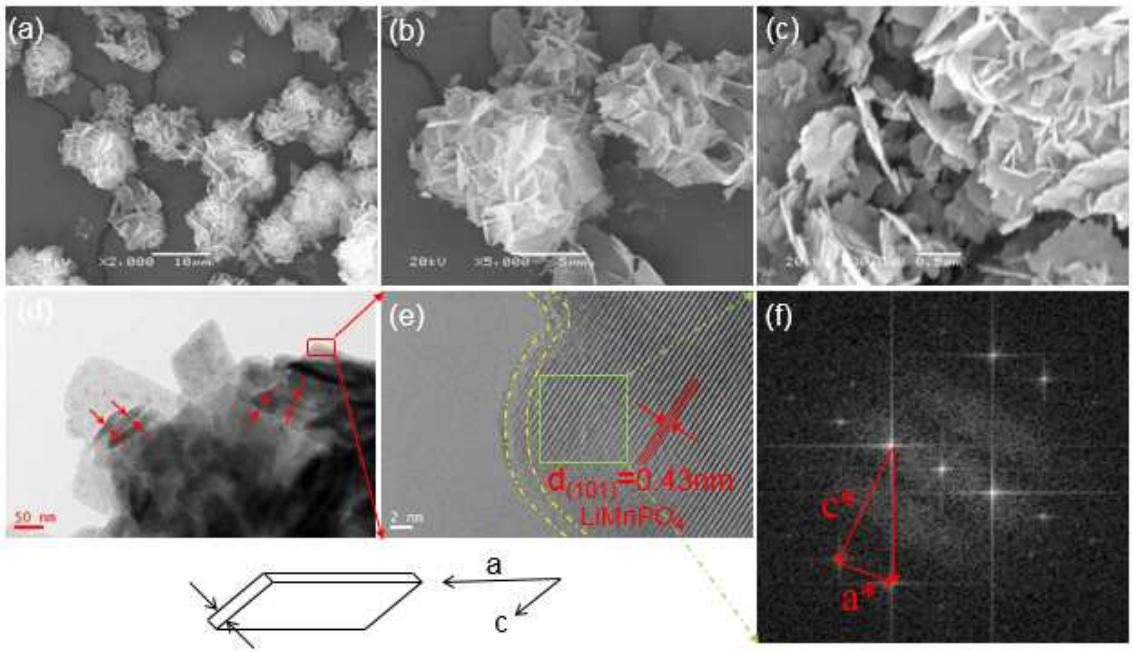

Fig. 6 the morphology of the flower-like $LiMnPO_4$: (a), (b), (c) the SEM images of $LiMnPO_4$; (d) the TEM images of $LiMnPO_4$/C; (e) the HRTEM images from the red region of (d); (f) the FFT of the off-green region of (e)

3.3 electrochemical performance

The electrochemical performance of the as-prepared $LiMnPO_4$ cathode materials with various morphology and particle size

RSC Advances Accepted Manuscript

was studied for its potential as a cathode material for lithium-ion batteries. Fig. 7a shows the typical discharge profiles of $LiMnPO_4$/C at 0.1 C, in the voltage range of 2.5~4.5 V. All the $LiMnPO_4$/C exhibits a single discharge plateau around 4.0~4.1 V, corresponding to the redox couple of Mn^{3+}/Mn^{2+}, in well agreement with the typical lithium extraction-insertion reaction in pure olivine $LiMnPO_4$ phase. During the initial charge-discharge process, the flower-like $LiMnPO_4$/C demonstrates a reversible capacity of 150.4 mAh g^{-1}, while 126.3, 128.0, 130.0, 110.2 mAh g^{-1} for s-1, s-2, s-3, s-7, respectively. Obviously, the flower-like $LiMnPO_4$/C exhibits the longest and the most stable plateau with a highest discharge potential of about 4.1 V vs Li^+/Li, which indicates that the flower-like $LiMnPO_4$/C has the best reversibility of electrode reaction by reducing electrode polarization owing to the novel morphology with (010) facet exposed. In particular, the sample s-7 shows the shortest plateau with a discharge potential of about 4.0 V, while no other plateau related to the impurity phase is observed. The rate performance of the typical samples are presented in Fig. 7b. The cells are tested at various rate from 0.1 C to 2.0 C. It is noted that the flower-like sample shows a superior rate capacity, in particular at high rate, for example, it exhibits 125.5, 118.6 mAh g^{-1} at 1.0 C, 2.0 C, respectively. As for s-7, the sample shows the worst electrochemical performance, showing a capacity of 65.2, 50.9 mAh g^{-1} at 1.0 C, 2.0 C, respectively, which is significantly influenced by the manganese oxide impurity phase. Thus, the amount of urea is a crucial parameter to control the electrochemical properties of $LiMnPO_4$ in terms of controllable impurity phase. As shown above, these samples excluding s-7 do not contain any impurity phases and differ only in their morphology, particle size and crystal orientation. Therefore, we can imply that the morphology, particle size and crystal orientation play an important role in the electrochemical performance. In terms of the flower-like sample, it has such advantages listed below: (1) the as-prepared porous nanoparticles with the 3D hierarchical structure are beneficial to reduce the Li^+ diffusion pathway, and favorable to the full permeability and infiltration between electrolyte and active material; also, it can decrease the agglomeration, which has been a rather severe challenge to maintain the excellent performance; (2) the flower-like sample is composed of sheet-like nanocrystals with mainly (010) facet exposed, which has large facet in the a-c plane and is thin in the b axis, resulting in an increase in the electrochemical reaction surface area, and enhancement in electrical conductivity and Li^+ diffusion. (3) The well decorated carbon coating provides easy electron transfer, which is beneficial to improve the kinetic process. Thus, it is self-evident that the flower-like $LiMnPO_4$/C behaves superior electrochemical performance. The samples including s-1, s-2 and s-3 exhibit almost the same electrochemical performance due to the various morphology and structure. For example, s-1 has a desired exposed facet (010) with a relative thick nanosheets, while s-2 shows a less uniform particle size distribution. As the Li:Mn:P molar ratio increased further, the sample s-3 exhibits the spherical nanoparticles with smaller particle size. However, it exhibits agglomeration to some degree, which is adverse to the effective contact between electrolyte and active material, as well as additive Super P carbon between nanoparticles during the fabrication of the composite electrodes. In addition, the mainly exposed facet is different with the (010). In a word, the electrochemical performance of $LiMnPO_4$ is significantly affected by the morphology and structure.

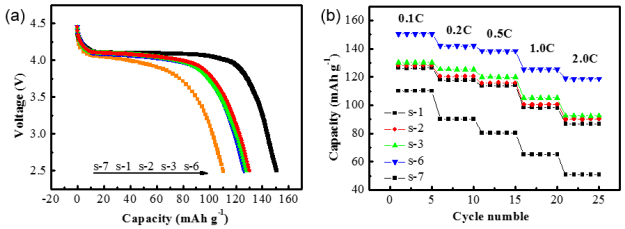

Fig. 7 the electrochemical performance of the typical $LiMnPO_4$/C samples: (a) the initial discharge curve at 0.1 C; (b) the rate capacity from 0.1 C to 2.0 C

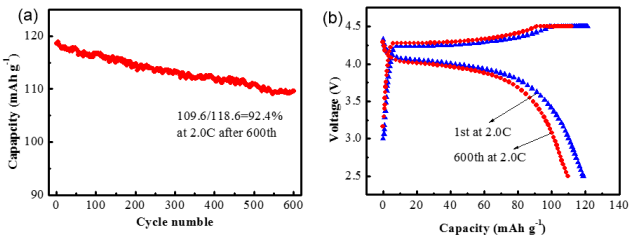

Fig. 8 the cycle performance of the flower-like $LiMnPO_4$/C: (a) the cycle curve at 2.0 C for 600th; (b) the charge-discharge profile after 1st and 600th

Long cycle performance is one of the significant electrochemical aspects of lithium-ion batteries for high power applications. The cycle performance of the flower-like $LiMnPO_4$/C is shown in Fig. 8a. The cells were cycled at 2.0 C in the voltage range of 2.5~4.5 V. As shown in Fig. 8b, the initial discharge capacities of $LiMnPO_4$ sample is 109.6 mA g^{-1} with a potential plateau of about 4.0 V. As usual, upon increasing the cycle number, the samples exhibit slight polarization, which is reflected in the term of potential difference between the charge-discharge plateaus, thereby declining the storage capacity of the electrode. However, the flower-like sample displays excellent cycle stability with a negligible voltage fading after 600 cycles at 2.0 C, showing a capacity retention up to 92.4%, which indicates that those novel morphology can obviously improve the cycle behaviour, especially at high rate.

Conclusions

In summary, we successfully synthesized the $LiMnPO_4$ nanoparticle with different morphology and particle size via solvothermal method. The results show that morphology and particle size was controllable synthesized with various precursor composite tailoring with the molar ratio of Li:Mn:P.

RSC Advances Accepted Manuscript

This journal is © The Royal Society of Chemistry 20xx

From 2:1:1 to 3:1:1, the particle morphology evolves from sheet-like to spherical texture while the particle size reduced, accompanied with the phase composition from Mn^{2+}-containing precursor to Li^{+}-containing precursor. In addition, the urea is used to further confirm the conclusions, in which the urea has no obvious effect on the morphology, but prevent crystals from growing and reduce the agglomeration. At the concentration of 0.16 mol L^{-1}, the sample consists of small sheet-like crystals with flower-like texture, delivering excellent reversible capacity of 150.4, 125.5, 118.6 mAh g^{-1} at 0.1, 1.0, 2.0 C, respectively. The composites show long cycle stability at high rate, displaying a capacity retention up to 92.4% with no apparent voltage fading after 600 cycles at 2.0 C. The attracting electrochemical performance of the flower-like $LiMnPO_4$/C composites suggests that the unique 3D hierarchical structure with (010) facet exposed and well carbon decorated is a promising way for high power Li-ion batteries electrode materials. Combination of the simple and facile synthesis method, it may also be applicable for the other olive type cathode materials such as $LiFePO_4$, $LiCoPO_4$ that require electrodes with high electronic and ionic conductivity.

Acknowledgements

This work was supported by the Nature Science Foundation of Hunan province (Grant No.2015JJ3152), Fundamental Research Funds for the Central Universities (2012QNZT018), and China Postdoctoral Science Foundation (2012M521546).

Notes and references

1. A. K. Padhi, K. S. Nanjundaswamy and J. B. Goodenough, *J. Electrochem. Soc.*, 1997, **144**, 1188-1194.
2. M. Yonemura, A. Yamada, Y. Takei, N. Sonoyama and R. Kanno, *J. Electrochem. Soc.*, 2004, **151**, A1352-A1356.
3. C. Delacourt, L. Laffont, R. Bouchet, C. Wurm, J. B. Leriche, M. Morcrette, J. M. Tarascon and C. Masquelier, *J. Electrochem. Soc.*, 2005, **152**, A913-A921.
4. D. Arčon, A. Zorko, P. Cevc, R. Dominko, M. Bele, J. Jamnik, Z. Jagličić and I. Golosovsky, *J. Phys. Chem. Solids*, 2004, **65**, 1773-1777.
5. A. Yamada, M. Hosoya, S.-C. Chung, Y. Kudo, K. Hinokuma, K.-Y. Liu and Y. Nishi, *J. Power. Sources*, 2003, **119-121**, 232-238.
6. N. H. Kwon and K. M. Fromm, *Electrochim. Acta*, 2012, **69**, 38-44.
7. A. Vadivel Murugan, T. Muraliganth, P. J. Ferreira and A. Manthiram, *Inorg Chem*, 2009, **48**, 946-952.
8. Y. Wang, Y. Yang, Y. Yang and H. Shao, *Solid State Commun.*, 2010, **150**, 81-85.
9. F. Wang, J. Yang, P. Gao, Y. NuLi and J. Wang, *J. Power. Sources*, 2011, **196**, 10258-10262.
10. L.-e. Li, J. Liu, L. Chen, H. Xu, J. Yang and Y. Qian, *RSC Adv.*, 2013, **3**, 6847-6852.
11. J. Liu, X. Liu, T. Huang and A. Yu, *J. Power. Sources*, 2013, **229**, 203-209.
12. J. Su, B.-Q. Wei, J.-P. Rong, W.-Y. Yin, Z.-X. Ye, X.-Q. Tian, L. Ren, M.-H. Cao and C.-W. Hu, *J. Solid State Chem.*, 2011, **184**, 2909-2919.
13. X.-L. Pan, C.-Y. Xu, D. Hong, H.-T. Fang and L. Zhen, *Electrochim. Acta*, 2013, **87**, 303-308.
14. Z. Dai, L. Wang, F. Ye, C. Huang, J. Wang, X. Huang, J. Wang, G. Tian, X. He and M. Ouyang, *Electrochim. Acta*, 2014, **134**, 13-17.
15. K. Dokko, S. Koizumi, H. Nakano and K. Kanamura, *J. Mater. Chem.*, 2007, **17**, 4803-4810.
16. L. Hu, B. Qiu, Y. Xia, Z. Qin, L. Qin, X. Zhou and Z. Liu, *J. Power. Sources*, 2014, **248**, 246-252.
17. Z. Dai, L. Wang, X. He, F. Ye, C. Huang, J. Li, J. Gao, J. Wang, G. Tian and M. Ouyang, *Electrochim Acta*, 2013, **112**, 144-148.
18. D. Fujimoto, Y. Lei, Z.-H. Huang, F. Kang and J. Kawamura, *Int. J. Electrochem.*, 2014, **2014**, 1-9.
19. D. Wang, H. Buqa, M. Crouzet, G. Deghenghi, T. Drezen, I. Exnar, N.-H. Kwon, J. H. Miners, L. Poletto and M. Grätzel, *J. Power. Sources*, 2009, **189**, 624-628.
20. K. Dokko, S. Koizumi, K. Sharaishi and K. Kanamura, *J. Power. Sources*, 2007, **165**, 656-659.
21. K. Dokko, T. Hachida and M. Watanabe, *J. Electrochem. Soc.*, 2011, **158**, A1275-A1281.
22. Z. Li, K. Zhu, J. Li and X. Wang, *CrystEngComm*, 2014, **16**, 10112-10122.
23. B. Ellis, W. H. Kan, W. R. M. Makahnouk and L. F. Nazar, *J. Mater. Chem.*, 2007, **17**, 3248-3254.
24. J. Chen, J. Bai, H. Chen and J. Graetz, *J. Phys. Chem. Lett.*, 2011, **2**, 1874-1878.
25. K. Dokko, K. Shiraishi and K. Kanamura, *J. Electrochem. Soc.*, 2005, **152**, A2199-A2202.
26. K. Shiraishi, K. Dokko and K. Kanamura, *J. Power. Sources*, 2005, **146**, 555-558.
27. C. M. Burba and R. Frech, *J. Electrochem. Soc.*, 2004, **151**, A1032-A1038.
28. M. S. Islam, D. J. Driscoll, C. A. J. Fisher and P. R. Slater, *Chem. Mat.*, 2005, **17**, 5085-5092.
29. C. Ouyang, S. Shi, Z. Wang, X. Huang and L. Chen, *Phys. Rev. B*, 2004, **69**, 104303.

RSC Advances Accepted Manuscript

Journal Name

ARTICLE

Table of content entry

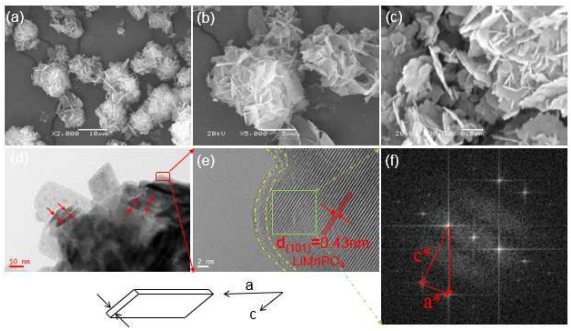

The hierarchical flower-like $LiMnPO_4$/C micro-nanostructures with (010) exposed and uniform carbon coated were prepared to provide a superior Li^+ migration and electron transfer via the solvothermal method with the assisted of urea. The as-prepared material showed excellent high rate capacity, and behaved long cycle performance.

RSC Advances Accepted Manuscript